ELSEVIER

Journal of Molecular Structure (Theochem) 585 (2002) 105–117

THEO CHEM

www.elsevier.com/locate/theochem

Exploring the potential energy surface of the ethyl cation by new procedures

Wolfgang Quapp[a,*,1], Dietmar Heidrich[b]

[a]*Mathematisches Institut, Universität Leipzig, Augustus-Platz, D-04109 Leipzig, Germany*
[b]*Wilhelm-Ostwald-Institut für Physikalische und Theoretische Chemie Universität Leipzig, Johannisallee 29, D-04103 Leipzig, Germany*

Received 5 October 2001; revised 7 January 2002; accepted 7 January 2002

Abstract

The MP2/6-31G** potential energy hypersurface (PES) of the chemically interesting molecule ion, $C_2H_5^+$, is analyzed by new procedures proposed by us recently. The reaction paths (RPs) start from the minima or saddle points by following the so-called reduced gradient procedure and/or its modification, the tangent search concept (TASC). The minimum energy paths (MEP) obtained by TASC are fine approximations of those gradient extremals, which follow the valley floor (or ridge) along the smallest (absolute) eigenvalue of the Hessian. It is the valley floor gradient extremal which is also termed the streambed of the PES. Tracing the streambed uphill we locate saddle points of the H-scrambling in $C_2H_5^+$. The potential energy surface of this cation is used to systematically explore the properties of RP definitions with particular focus to RP bifurcations. The intrinsic reaction coordinate (IRC), which is mostly used as MEP in chemistry, is included for the purpose of comparison.

Keywords: H-scrambling; Reaction path following; Valley-ridge-inflection points; Bifurcation points; Saddle points

1. Introduction

The particular chemical interest for the ethyl cation is due to the fact that first it is the smallest cation which can be formed by protonation of a double bond, and second its equilibrium structure forms a nonclassical structure in the gas phase. In other words, the competition between classical (**2**, C_s) and nonclassical (**1**, C_{2v}) structures (see Fig. 1) shows the nonclassical one in favor in contrast to the situation in (nucleophilic) solvents. The first calculations establishing the larger stability of **1** were given by Zurawski et al. using the IEPA PNO procedure to include electron correlation [1]. With the more sophisticated CEPA method the relative stabilities were confirmed [2] in 1977 and the energy difference ΔE_{pot} (**2** − **1**) was estimated to be somewhat smaller than 7.3 kcal/mol. Some experimental findings are available. They support these results, cf. Ref. [3]. The survey [3] also shows high sophisticated ab initio energy differences ΔE_{pot} (**2** − **1**) ranging from 4.7 to 8.4 kcal/mol.

The considerable success of quantum chemistry in predicting the ethyl cation structure in the gas phase

* Corresponding author. Tel.: +49-341-97-32153; fax: +49-341-97-32199.
E-mail address: quapp@rz.uni-leipzig.de (W. Quapp).
[1] Web: http://mathematik.uni-leipzig.de/MI/quapp/.

Abbreviations: BP, bifurcation point (of a curve); EV, eigenvector; GE, gradient extremal; IRC, intrinsic reaction coordinate; MEP, minimum energy path; MIN, Minimum (of PES); PES, potential energy hypersurface; RGF, (method of) reduced gradient following; RP, reaction path; SP, saddle point (of PES); TASC, (method of) tangent search concept; VRI, valley-ridge-inflection (point of PES)

0166-1280/02/$ - see front matter
PII: S0166-1280(02)00037-4

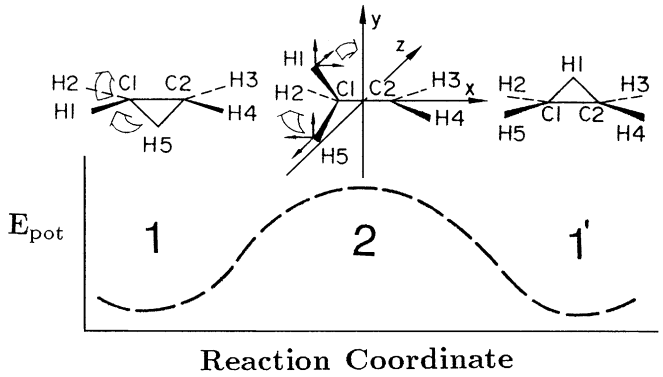

Fig. 1. Description of the proton shift in the ethyl cation along the MEP [4]; **1**, **1**′ nonclassical (C_{2v}) and **2** classical (C_s) structures.

was connected with the quantum chemical findings that only correlated levels of theory are able to give correct predictions for structures of carbocations. Gradient procedures of geometry optimization and vibrational analyses were first used to identify the stationary structures **1**, **2** in 1976 [2,4]. These calculations used the fact that certain semi-empirical methods could reproduce the classical–nonclassical energy difference found by correlated ab initio methods. The calculation of the reaction path (RP) of the H-shifts shows **2** to be the SP of the proton shifts, see Fig. 1(taken from Ref. [4]).

In solution the solvents may stabilize **2** by nucleophilic interactions with the positive charge of the sp^2-carbon center. In the isolated ethyl cation the following chemical processes are of particular interest:

(i) the RP of hydrogen shifts (H scrambling),
(ii) H_2 lost to give the vinyl cation (protonated acetylene), cf. [5,6], and
(iii) other dissociation processes.

These pathways are accompanied by bifurcations of the MEP which we treat for points (i) and (ii). This paper aims at the demonstration of the possibilities of the combined use of new and 'classical' methods of PES analysis.

The underlying concept of the MEP or RP of a PES is the usual approach to theoretical kinetics of larger chemical systems [7–10]. It is able to describe pathways of conformational rearrangements as well. The RP is defined as the line in the configuration space which connects the reactant and the product minimum by passing the SP of the PES. The SP (the transition structure) and the minima form stationary points of the PES. The mathematical description of a MEP turned out to be more difficult than expected [11]. We use different mathematical RP definitions: steepest descent (IRC), the 'reduced gradient following' (RGF) [12–14], and the valley ground gradient extremal (GE) [15,16] or its low order approximation TASC [17,18]. One has to insist upon that the different RP definitions may lead to different curves; although these definitions are chosen independently of the coordinate system used. The independence on the coordinate system was shown for the IRC [11], and for the GE, as well [19]. A particular aspect is the computation of RP branching (bifurcation) using calculations of valley-ridge-inflection (VRI) points by the Branin method [13,14,20] and the determination of GE bifurcation [15,16]. It should be noted that the calculation of VRI points is developed in a coordinate independent definition [21,22].

All these detailed activities for a simple and exact calculation of RPs are prerequisites for a number of dynamical theories to come into operation, including the famous RP Hamiltonian [8,9]. Further, the methods of direct dynamics [10,23,24] need an exact and physically sensible description of the RP [25,26]. One point of particular interest is that the knowledge of the reaction pathways may give tools for the interpretation of infrared spectra of vibrationally highly excited molecules [14] and for the prediction of the conditions of mode selective reactions.

The paper is organized as follows: First, we shortly

repeat the mathematical fundamentals of the RGF method [12–14], and define a modified RGF by the 'tangent search concept' (TASC) [17,18]. It has a close connection to the streambed gradient extremal [27]. Subsequently, the successful finding of reaction pathways and stationary points as well as VRI points on RPs is demonstrated.

The methods are implemented as subroutine in our research code of the GAMESS-UK program [28], as well as independent modular programs. The programs can be obtained on request or downloaded [1].

2. Theoretical methods of PES analysis

We use an arsenal of different methods to follow static RPs. The first one is the well known IRC [29], cf. also Ref. [11]. The favored method used in this paper is the so-called RGF [12–14], a very effective revisal of the old distinguished coordinate method [30]. Equivalent curves are obtained by the global Newton method (the Branin trajectories [20]). Branin's method is additionally well adapted to exactly calculate VRI points [13]. A recent development is the TASC method [17,18] which allows calculating valley floor gradient extremals by second order methods only. If stationary points are found by RGF or TASC, they are refined by the full-matrix Newton–Raphson method. A steepest descent run is used to prove the direct connection between the SP and the minimum.

2.1. IRC

Be $E(\mathbf{x})$ the function of the PES, and be $\nabla E(\mathbf{x})$ its gradient vector, $\mathbf{g}(\mathbf{x})$, in the configuration space, $\mathbf{R}^n$, which is defined by the coordinates $\mathbf{x}$ of the molecule. As usual, $n = 3N - 6$ forms the number of independent internal coordinates being the dimension of the problem. $\mathbf{x}$ and $\mathbf{g}$ are vectors of this dimension n. The mass-weighted steepest descent starts at a SP of index one a step in the direction of the decomposition vector. The steepest descent along the gradient, $-\mathbf{g}$, is calculated by discretizing the corresponding differential equation to

$$\mathbf{x}_{m+1} = \mathbf{x}_m - l\mathbf{g}_m \tag{1}$$

where m is the step number and l is a steplength parameter used to damp or accelerate the step. We do not use a corrector for the method. The steepest descent from a SP of index one gives the so-called IRC. The IRC is frequently used as synonym for the MEP of the PES. Note that in internal curvilinear coordinates we have to use the co- and contravariant versions of gradient and coordinate steps in Eq. (1), see Ref. [11].

2.2. RGF and tangent search concept

RGF finds a curve where the selected gradient direction comes out to be fixed at every curve point, $\mathbf{x} = \mathbf{x}(t)$

$$\nabla E(\mathbf{x}(t))/\|\nabla E(x(t))\| = \mathbf{r} \tag{2}$$

where t is the curve parameter, and $\mathbf{r}$ is the unit vector of the fixed search direction [13]. The search direction usually corresponds with the start direction of a chemical reaction. The resulting curves pass all stationary points of the PES in most cases. Thus, RGF is a simple but effective procedure in order to determine all types of stationary points [12]. Unlike the steepest descent path from a saddle, the reduced gradient search for a fixed direction has locally an explicit analytical definition: Eq. (2). In other words, the difference between the two kinds of curves is that RGF along direction $\mathbf{r}$ does not give a curve through every point. However, a steepest descent trajectory is going through every point. We recall that RGF curves are not generally minimum energy pathways [12,31]. The RGF curve (2) may be near to a valley floor line or not. Nevertheless, these curves may follow a RP in favorable cases, at least qualitatively. The possibility of the MEP calculation then depends on a clever definition of the search direction [32].

To realize the requirement (Eq. (2)), the RGF algorithm [13] uses a projection of the gradient of the PES to fulfill the equations

$$\mathbf{P}_\mathbf{r}\mathbf{g}(x(t)) = \mathbf{0} \tag{3}$$

where the projector may be defined by the dyadic product

$$\mathbf{P}_\mathbf{r} = \mathbf{I}_n - \mathbf{r}\mathbf{r}^T \tag{4}$$

which realizes $\mathbf{P}_\mathbf{r}\mathbf{r} = \mathbf{0}$. $\mathbf{g}$ and $\mathbf{r}$ are column vectors, $\mathbf{I}_n$ is the unit matrix in n dimensions, where $\mathbf{r}^\mathrm{T}$ with the upper index T means transposition to a line vector. Thus, $\mathbf{r}\mathbf{r}^\mathrm{T}$ is a matrix. This results in the zero vector of the reduced gradient (3). The projector, $\mathbf{P}_\mathbf{r}$, is a

constant matrix of rank $(n-1)$: that one which enforces the gradient to point at every curve point, $\mathbf{x}(t)$, into the same direction $\mathbf{r}$. The tangent to curve (3), $\mathbf{x}'(t)$, is obtained by a solution of the following system of equations:

$$\frac{\mathrm{d}}{\mathrm{d}t}[\mathbf{P}_\mathbf{r}\mathbf{g}(\mathbf{x}(t))] = \mathbf{P}_\mathbf{r}\frac{\mathrm{d}\mathbf{g}(\mathbf{x}(t))}{\mathrm{d}t} = \mathbf{P}_\mathbf{r}\mathbf{H}(\mathbf{x}(t))\mathbf{x}'(t) = \mathbf{0} \tag{5}$$

where $\mathbf{H}$ is the Hessian of the PES. The simplicity of the RGF method is based on the constance of the $\mathbf{P}_\mathbf{r}$ matrix. The predictor–corrector method of RGF implies the predictor step along the tangent $\mathbf{x}'(t)$, and, orthogonally to this direction, Newton–Raphson steps of the corrector for a solution of curve (3).

We modified RGF to search for MEPs [17,18]. The constant search direction $\mathbf{r}$ in Eq. (3) of the RGF method is replaced by a direction which is changed during the iteration process. We utilized the tangent of the searched curve itself as new gradient direction. Each corrector step is calculated using the tangent direction of the previous predictor. This leads to self-consistency on the valley floor GE. The method is called the TASC. Details are given in Refs. [17,18]. TASC is limited to follow the direction of the smallest eigenvalue. Its success results from the self-correction property. The new method also works in cases where turning points of the streambed GE appear. Such regions are overcome by successive corrector steps. In general, the TASC curve follows the valley floor. It is simpler than the frontier mode-following [33] which attempts to find the valley direction 'by hand'. Using TASC, the diagonalization of the Hessian to calculate the lowest eigenvector is avoided. The aspect becomes computationally important for very large systems [34]. In contrast to the well-known method of eigenvector following [35–37], our method provides a locally defined curve, found by a predictor–corrector scheme. So, this pathway can be calculated as exactly as necessary by diminishing the steplength of the predictor and the threshold of the corrector. In this manner, the path forms a fine approximation of that MEP following the smallest ascent starting from the minimum.

2.3. Branin method

In our calculations the Branin method is used as follows: we choose by trial and error the steplength parameter, l, and discretize Branins differential equation [13,14,20,38] to

$$\mathbf{x}_{m+1} = \mathbf{x}_m \mp l\mathbf{A}_m\mathbf{g}_m \tag{6}$$

where m is the step number. $\mathbf{A}_m$ is the adjoint matrix of the Hessian and $\mathbf{g}_m$ is the gradient at point $\mathbf{x}_m$. For example, we used for calculating VRI points an l value varying between 0.0004 and 1.0. The value depends on matrix $\mathbf{A}_m$ as well as on the gradient $\mathbf{g}_m$ at $\mathbf{x}_m$, and sometimes it has to be adapted during the calculation for a satisfactory exploration along the Branin trajectory. The product of adjoint matrix times gradient in Eq. (6) becomes small near VRI points. This causes smaller steps near the VRI, and if the parameter l is appropriately chosen, then a good convergence is obtained. We do not need a corrector for the Branin method, because we are not interested in an exact curve following. In contrast, we search for the exact zero of the orthogonal eigenvalue of any Branin curve. Thus, the stopping criterion is the zero of the ridge eigenvalue: below the line of $1\ \mathrm{cm}^{-1}$ the algorithm stops.

2.4. Gradient extremals

If the norm of the gradient forms a minimum along points of an equi-subsurface, $f(\mathbf{x}) = \text{const.}$, i.e. along all directions perpendicularly to the gradient [39–41], a point of gentlest ascent of a valley is found. The measure for the ascent of the function $f(\mathbf{x})$ is the norm $\sigma(\mathbf{x})$ of the gradient vector. This results in the basic eigenvector relation

$$\mathbf{H}(\mathbf{x})\mathbf{g}(\mathbf{x}) = \lambda(\mathbf{x})g(\mathbf{x}). \tag{7}$$

The proportional factor $\lambda(\mathbf{x})$ is an eigenvalue of the Hessian, and the gradient is its eigenvector. Curves defined by Eq. (7) consisting of such points on consecutive equi-hypersurfaces are termed gradient extremals [40]. The GE Eq. (7) selects all points of the configuration space having an extreme value of the gradient norm $\sigma(\mathbf{x})$ with respect to variations on equi-hypersurfaces. If $\sigma(\mathbf{x})$ has a minimum, the energy function may show a valley-floor GE, however, it can also be a crest of a ridge. The extremes of $\sigma(\mathbf{x})$ may also be maxima or degenerate stationary points [15,41,42].

The streambed description of the valley ground

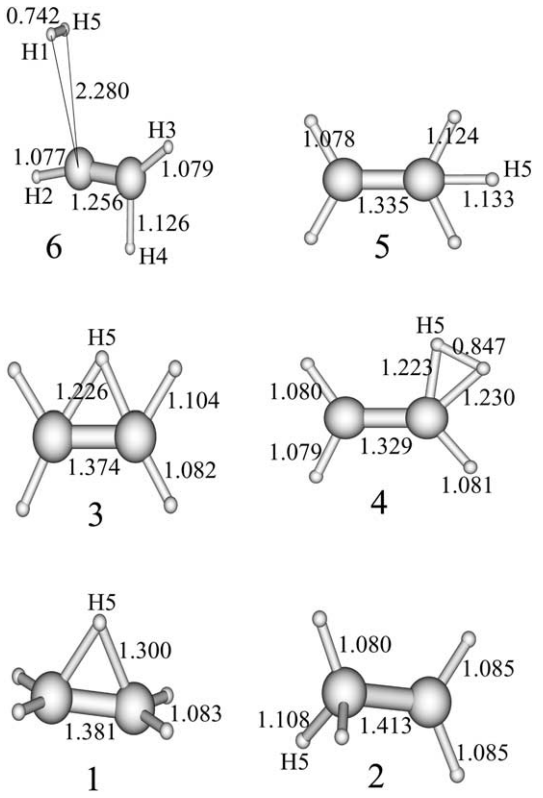

Fig. 2. The geometry of six stationary structures of $C_2H_5^+$ with the MP2/6-31G** method, plotted by Molden [43]. The distances are given in Å. Structures **2**, **4**, and **6** are SPs of index one, but the SPs **3** and **5** are of index two. Structures **3**, **4**, and **5** are planar.

Table 1
Normal modes of MIN **1**, SP **2**, and SP **6** of $C_2H_5^+$ in cm^{-1}

No	Sym	MIN	Sym	SP **2**	Sym	SP **6**
1	B2	763	A″	367i	A″	407i
2	B1	865	A″	766	A″	238
3	A2	1113	A′	828	A′	239
4	B1	1156	A′	1118	A′	299
5	A1	1177	A′	1227	A″	361
6	A2	1291	A′	1304	A″	477
7	B2	1347	A″	1315	A″	667
8	A1	1398	A′	1444	A″	812
9	B2	1527	A′	1503	A′	1054
10	A1	1626	A′	1614	A′	1194
11	A1	2273	A′	2994	A′	1859
12	B2	3234	A″	3015	A′	2896
13	A1	3237	A′	3221	A′	3337
14	A2	3351	A′	3319	A′	3423
15	B1	3366	A′	3344	A′	4456

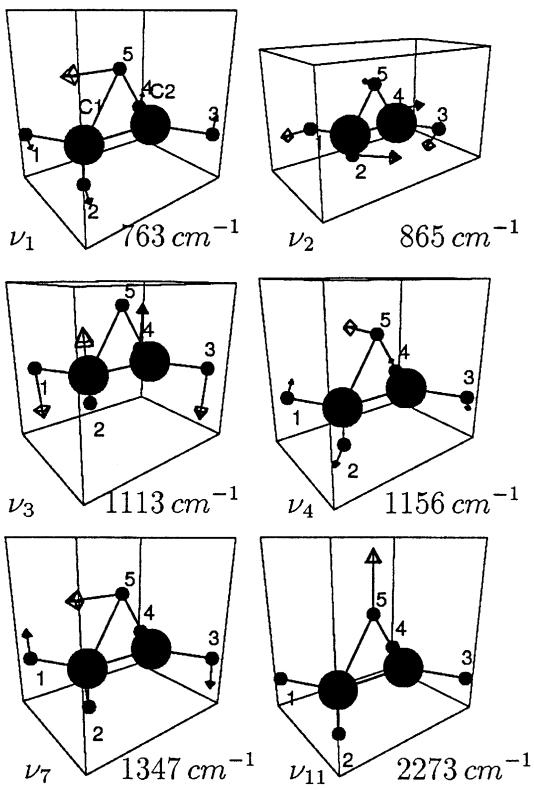

Fig. 3. Normal modes of $C_2H_5^+$ at the **minimum 1** with MP2/6-31G** drawn by Mathematica.

gradient extremal is founded on the property to follow the smallest eigenvalue direction. Being on this gradient extremal, from the left, as well as from the right hand side the steepest descent lines are confluent to the valley line.

3. Results of the calculation of the electronic ground state PES of $C_2H_5^+$

3.1. Minimum and lowest SP

The theoretical calculations [1,2] show that the nonclassical singly bridged structure **1** (C_{2v}) is the global minimum. Classical forms $H_3C–CH_2^+$ collapse into the bridged form as soon as correlation effects are taken into account. The classical form **2** is a SP for the intramolecular hydrogen shift, see below.

Fig. 2 shows the geometries of the equilibrium structure and of further stationary points of $C_2H_5^+$. In

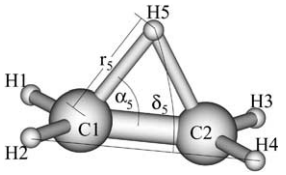

Fig. 4. Some internal coordinates used in the calculation of $C_2H_5^+$.

this study, we use the MP2/6-31G** method [44] for all calculations of the potential energy, the gradient and Hessian. The method is well suited to give a realistic representation of the PES of the ethyl cation. The difference ΔE_{pot} (**2** − **1**) is calculated to be 7.6 kcal/mol with a somewhat smaller difference at 0 K, $\Delta E_0 = 6.60$ kcal/mol. (The first estimation of the zero-point vibrational energy differences was given in Ref. [45].)

It is obvious that the quantum chemical level used is not sufficient to give a PES of $C_2H_5^+$ which is correct

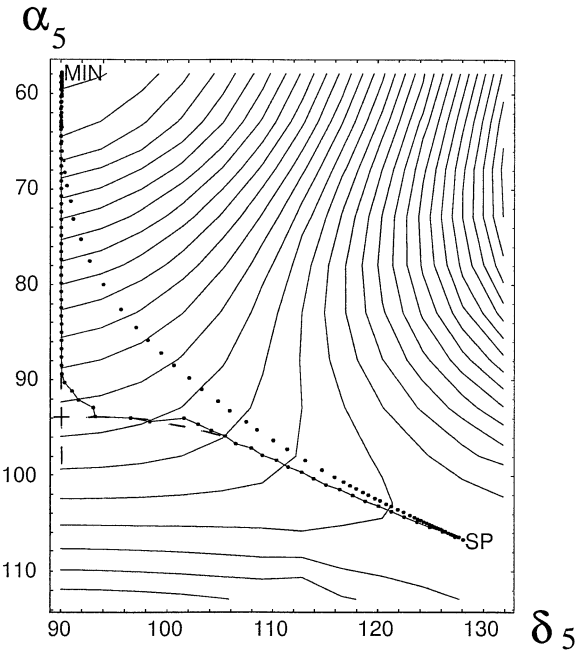

Fig. 5. MP2/6-31G** potential surface of $C_2H_5^+$: at a grid of 12 × 12 points of fixed H5 angles, α_5 and δ_5, the other coordinates are optimized. The dotted line uphill from minimum (MIN) to SP at $(\alpha_5, \delta_5) = (106, 128°)$ shows the 'H-shift channel'. It is composed by two streambed GEs and was found by TASC. TASC branches near 89.3° and finds the beginning of the second GE valley (up to the SP) by corrector steps. In contrast, the IRC downhill from the SP is depicted by dots only. The bifurcation of the GE at 94° is depicted by dashes.

in all details, especially the description of the dissociation channels is a rough estimate. However, the main parts of the PES covering the classical–nonclassical cation range are expected to be reliably reflected. We know that the H_2 lost $C_2H_5^+ \rightarrow C_2H_3^+ + H_2$ should be better described by methods considering dynamical correlation. It is not the objective of this paper to give a highest level description of the high-energy parts of the PES. Here, the MP2 ab initio PES of the ethyl cation is used as model surface.

In Table 1 the normal mode frequencies of $C_2H_5^+$ at the global minimum **1** and at SP **2** are listed. Fig. 3 shows selected normal modes of the minimum. These are those modes (without ν_3) which have concern to the bridged H5 in structure **1**: the modes ν_1 at 763 cm^{-1}, ν_2 at 865 cm^{-1}, ν_3 at 1113 cm^{-1}, ν_4 at 1156 cm^{-1}, ν_7 at 1347 cm^{-1}, and ν_{11} at 2273 cm^{-1}.

The lowest mode, ν_1, thus the direction of the MEP leaving the minimum, is the ring opening mode of H5 in the C_s symmetry plane.

We depicted the corresponding angle coordinate by α_5, see Fig. 4. With TASC, we followed this RP of a GE along the first mode of the H5. In addition we used this pure ring opening coordinate of H5 as the search direction for an RGF approximation of the MEP. The PES analysis is shown by a surface section as given in Fig. 5. The contours are drawn with the help of 'Mathematica'. The axes are the H5 dihedral bending angle, δ_5, (against the remainder of the cation), and the H5 bending angle, α_5, of the bonds C1–H5 to C1–C2 generating the ring opening. The other coordinates are optimized in each of the 12 × 12 raster points.

The two pathways shown are calculated in the full 15-dimensional coordinate space of the molecule. They are projected into the sectional plane of Fig. 5. Note: a relaxed section through the 15-dimensional curvilinear coordinate space may be misleading! The calculation of the section of Fig. 5 is a 2D surface with two 'distuingished coordinates' [30,42]. It is a common misconception that the structure of a multidimensional PES can be determined by calculating and displaying the PES versus two coordinates, where the PES has been minimized with respect to the remaining coordinates. But here, the PES cut is founded on the fact that the two selected coordinates in Fig. 5 represent the dominant geometric changes along the MEP. This allows to assume that our choice is adapted to elucidate the vibrational behavior of the

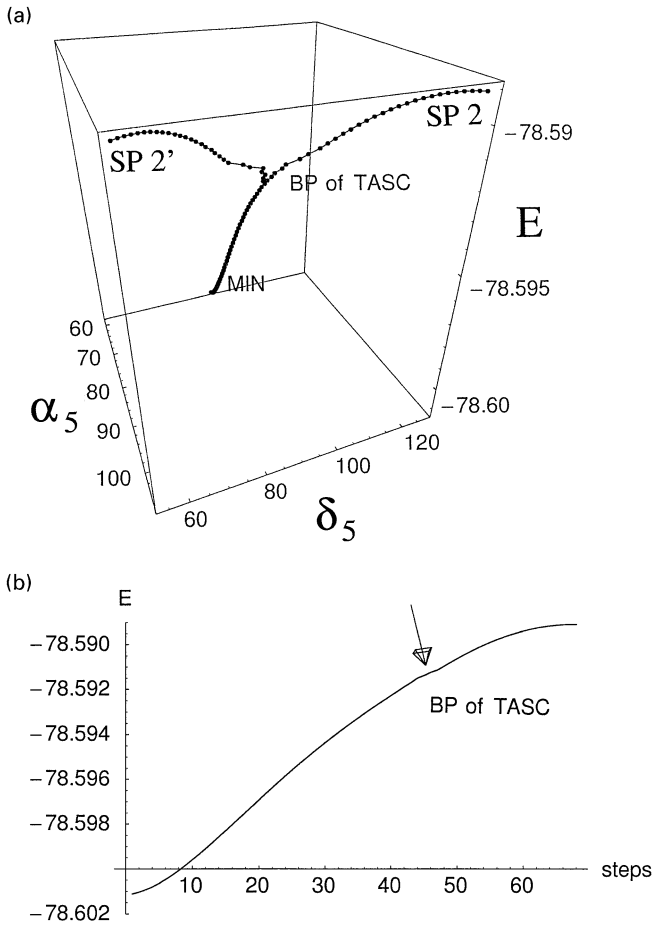

Fig. 6. (a) TASC potential energy profile of the H-shift in $C_2H_5^+$ with minimum **1** (MIN), SPs **2**, **2′** (SP) and the bifurcation point (BP). The plane of coordinates is the same as in Fig. 5, but symmetrically mirrored in δ_5. The bifurcation and the two symmetric branches of the pathways to two equivalent SPs are shown. (b) Potential energy profile of the 'reaction coordinate' found by TASC (predictor steps with fixed step length). At step 46 TASC changes the direction (in the plane of Fig. 5): the H5 ring opening angle is replaced by a concerted dihedral change of H5 and H1 up to the SP (at step 68) where both dihedrals are symmetric. Note: in this customary description, the change of the pathway direction at the BP is almost not detectable.

molecule. The curve obtained by TASC is visualized in Fig. 5 (connected dots) by projecting it into the figures plane. It is the pathway upslope along the 'scrambling channel' starting at the minimum up to the bifurcation. We may interpret the curve to be a numerically determined RP approximation. The RP in the C_s symmetry corresponds to the valley floor GE of the smallest eigenvalue, therefore, we have a streambed GE, a 'GE channel' [27]. The difference of this bifurcating GE with the steepest descent from the SP (the IRC) is evident. (This contrasts with an 'other behavior' of the IRC in Ref. [46], Fig. 2.)

The TASC path is a composition of two pieces: first the H5 ring opening mode, and second, the quasi symmetric dihedral angles of H5 and H1 change out of plane into the end CH_3 group. There is an edge in the curve where the TASC curve changes the direction at $\alpha_5 = 89.3°$, and the two lowest eigenvalues of the Hessian change their relation. On the other hand, the IRC goes from the SP structure **2** curvilinear across the region for which the two pieces of TASC form the boundary of. The two kinds of curves (TASC or IRC) are both approximations of a static RP. Both kinds have their merits to give insights into molecular

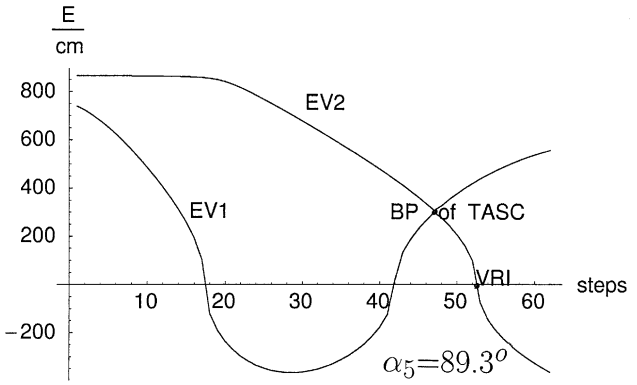

Fig. 7. The first two eigenvalues (EV) of $C_2H_5^+$ over a reduced gradient (RGF) search pathway, up to the onset of a ridge after step 52, the VRI point. This pathway is the ordinate axis α_5 in Fig. 5 where the VRI point is at $\approx 103°$. The crossing of the two eigenvalues at $\approx 89.3°$ (step 46) is shown and leads to a sudden change in the direction of the TASC route.

behavior. TASC, with the crossing point of eigenvalues at 89.3°, representing the model line of the valley floor GE along the streambed (with a bifurcation point at 94°), generates features which are not indicated by the IRC.

Fig. 6 shows different views to the energy profile over the RP simulated by TASC. Fig. 6(a) is a perspective view of the TASC pathway between the global minimum **1** and the SP **2** (or the analogous SP **2**′ where H2 moves and δ_5 decreases) drawn over the coordinate plane of Fig. 5. Both branches of the symmetry breaking are shown.

Fig. 6(b) shows the TASC energy profile depicted over an axis of the usual reaction coordinate description. The edge at 89.3° from Fig. 6(a), being the bifurcation to one of the SPs **2** or **2**′, is represented here (at step 46) by a weak shoulder which is nearly flattened out in this representation.

The IRC coming downhill from SP **2** confluences into the lowest mode direction at the α_5 axis of Fig. 5 in an asymptotic manner. Hence, we cannot discover the bifurcation structure of the PES by using the IRC only. This is even more of importance for unsymmetric systems and the next challenge for PES analysis. The GE direction along the α_5 axis is a normal mode direction of the vibrating molecule. The GE bifurcation at $\alpha_5 = 94°$ is sketched by dashes.

3.2. The process of the H-atoms scrambling

The SP **2** is the transition structure for the hydrogen shift. The potential energy barrier with the MP2/6-31G** method is about 7.6 kcal/mol. The equivalent SPs allow the bridged protons in the system to interchange their positions (cf. Fig. 1). In Fig. 5, the SP **2** is formed by the H1 atom, which is selected for the first act of scrambling. The direction of the decomposition vector at SP **2** depends on a linear combination of all eigenvectors of the minimum. If **v** is the mass weighted decomposition vector of the SP, and if $\mathbf{e}_i$ are the mass weighted eigenvectors of the minimum, the coefficients $\mathbf{v}\cdot\mathbf{e}_i$ for $i = 1,\ldots,15$ are (0.327, 0.270, 0.182, 0.151, 0.110, 0.306, 0.394, 0.027, 0.083, 0.169, 0.023, 0.234, 0.227, 0.170, 0.173). Thus, looking for a vibrational combination mode which explores the possible pathway to SP **2**, it is difficult to propose an appropriate choice of such a combination mode which may directly follow the way up to the SP. There is no spectroscopic study with respect to the H-shifts of $C_2H_5^+$ (experimental results indicate that the bridged structure is actually the equilibrium structure [47]).

3.3. The valley-ridge-inflection belt of the hydrogen shifts around the C_s minimum bowl

The symmetry breaking bifurcation of the streambed GE takes place at 94° along the H5 ring opening coordinate, cf. Fig. 5 where the GE bifurcation is sketched by dashes. However, with respect to the formation of normal modes, a GE bifurcation has no consequences as long as the GE still remains in the convex region of the corresponding PES plane, in

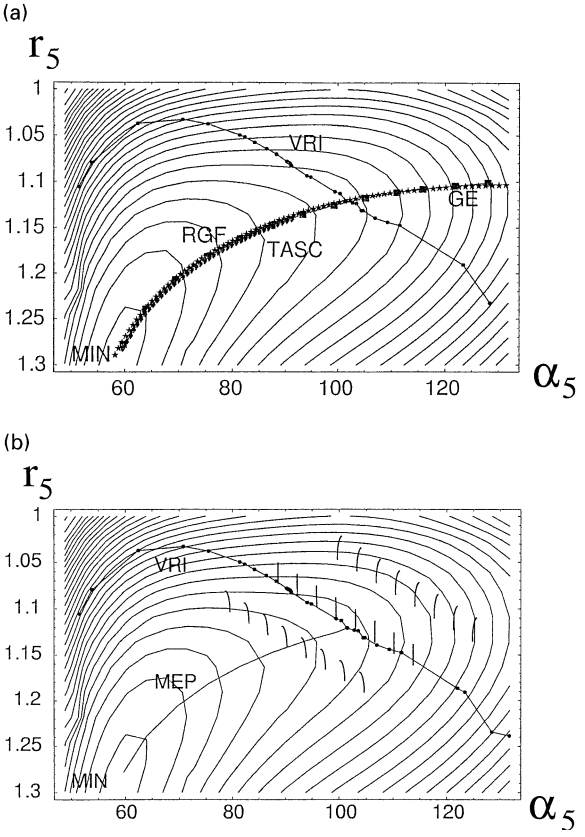

Fig. 8. (a) $C_2H_5^+$ potential energy surface (MP2/6-31G**) in a section from a grid of 24×12 points. A raster of H5 angles, α_5, and H5–C1 distances, r_5, is fixed, where all other coordinates are optimized. The dots are VRI points (connected by a polygon line). They begin in our calculation at (57°,1.115 Å), they cross the MEP at VRI (103°,1.12 Å), and they end in our calculation at the VRI at (131.4°, 1.225 Å). Approximations of the MEP by three full dimensional path following methods are given: the direct GE calculation (full squares), the TASC (full diamonds), and the RGF in direction of the pure ring opening of H5 (stars). The steplength is 0.25 for the GE, and 0.025 for TASC and RGF, where the corrector threshold is 0.00001 for all three calculations. (b) In this schematic sketch using the PES (a), the curvature of the corresponding level lines along the orthogonal eigenvector direction of the zero eigenvector of the VRI points is illustrated. The MEP of the full (15-dimensional) PES ends at least at the VRI belt and generates two branches leaving the plane selected here.

Fig. 5 at the α_5 axis up to 103°. More fundamental, and fortunately much cheaper to calculate, are the VRI points of the PES. They are defined by the zero eigenvalue of the eigenvector EV2 which is orthogonal to the gradient.

Fig. 7 shows the first two eigenvalues along the streambed GE (the H5 ring opening with α_5 in C_s symmetry). One eigenvalue concerns the curvature of this minimum energy pathway, the second is related to the next lowest curvature. The corresponding eigenvector is orthogonal to that of the GE. At the minimum (see Fig. 3), as well as at the VRI point, this second direction concerns partly the H5 dihedral change δ_5 and asymmetric changes of the other H atoms. The first interesting feature is the crossing of the two eigenvalues after step 46 (at an angle α_5 of H5 of 89.3°): there the streambed character of the GE ends; it continues as the floor line of a cirque. (The TASC calculation there leaves the C_s plane, being in Fig. 5 projected onto the α_5 axis, and finds by corrector steps one of the side branches of the GE which leads to the SP structure **2**. This breaking out of TASC is depicted in Fig. 7 by BP of TASC).

The second interesting feature here is that along the α_5-axis the PES changes in a cirque, and finally, the eigenvalue of the eigenvector of the orthogonal direction becomes zero. It means that the valley structure of the GE cirque ends there at all. The emerging negative eigenvalue of one orthogonal direction indicates the beginning of the ridge between the two (symmetric branching) side GEs leading to SP **2** or its equivalent double SP **2′**, respectively. Usually, such a VRI point will be found with an RGF procedure. If a first VRI point is found (here at $\alpha_5 = 103°$ at 2550 cm^{-1} over the minimum **1**) by following the RGF curve along the H5 ring opening in the C_s plane, we can start to search for further VRI points in a nearby region by using the Branin method [13]. Note that Fig. 5 gives a 2D section of the full 15 dimensions of the molecule. If one changes other degrees of freedom (still under the symmetry constraint) one may get further VRI points. One important condition of the Branin method to work is the strict symmetry constraint. When starting anywhere in the coordinate space, a Branin curve may almost approach a VRI point, however, usually it turns off before finally reaching this point. This is shown in Ref. [13]. Because of the symmetry requirement for the Branin method, we constrain 6×2 coordinates to be equal, correspondingly, resulting in a Branin calculation related to a $(6 + 3) = 9$-dimensional symmetric subspace. In Fig. 5, the ordinate axis of angle α_5 of H5 belongs to this subspace. Thus, further eight dimensions still remain there for

a symmetric C_s disturbance of the molecule. The general behavior of Branin curves is: they connect stationary points of a different index, or they end in a VRI point.

Fig. 8 shows a projected region of VRI points, which are reached by H5 if ascenting from the global minimum **1**. VRI points are defined by $\mathbf{Ag} = 0$, $\mathbf{g}$ is the gradient with $\mathbf{g} \neq 0$, and $\mathbf{A}$ is the adjoint of $\mathbf{H}$. The situation is illustrated in Fig. 8(b). We draw the curvature of corresponding level lines in a schematic sketch, along the second orthogonal eigenvector direction. They come out of the PES section plane. Fig. 8(b) explains the zero curvature property of these eigenvectors in this PES region. The calculated VRI points are connected by a polygon for better visualization. Additionally, the given curve of VRI points is the projection of calculated VRI points (in nine symmetry coordinates) into the plane of this Fig. 8, where the VRI manifold itself is higher dimensional than the one-dimensional curve of this section: it can have a dimension of up to $(N - 2)$ if N is the dimension of internal coordinates [13,14]. The special C_s symmetry of H5 is still conserved along the trajectory of a Branin calculation Eq. (6) by symmetrization of the next step.

Fig. 8 demonstrates that any C_s-ring opening or stretching vibration of H5, or any combination mode between them in the C_s plane of the global minimum, has to meet a VRI point. Thus, considering real vibrations, they could become instable when reaching regions of the PES beyond the belt of VRI points. For the symmetric H5 ring opening (vibrating through the global minimum) we find symmetric VRI points at both walls of the PES, for the forward as well as the backward bending vibration. Thus, if the ridge emerges at the MEP, two symmetric side valleys arise at every side of the PES bowl, where a vibration of the H5 may climb up the mountains using two of the four valleys. If the ion is excited by sufficient energy it reaches one of the equivalent SPs **2**.

Additionally, in Fig. 8 the calculated approximations of the MEP by direct GE calculation [15,16], by TASC [17,18] up to the branching point at 89.3°, and by RGF [12,13] are shown. Note: the observed coalescence of GE and RGF pathways is due to the existence of the deep streambed; it emerges in the example more accidentally by the proper choice of the RGF search direction. But the conformity of TASC and GE is not surprising [17,18] because TASC gives the streambed GE as long as this GE follows the smallest eigenvalue of the Hessian matrix. Nevertheless, the first crossing of the pathways of RGF or GE with the VRI manifold strongly characterizes the bifurcation of the reaction valley.

The apparent 'corner cutting' of the paths near $\alpha = 70°$ is due to the scaling of the axes. Also, the left hand side of the Fig. 8 may give an erronous impression of the symmetric PES because the coordinates r_5 and α_5 are directed to the C1 atom, and not to the symmetry center of the molecule at minimum. The coordinates do not symmetrically describe the $C_{2\nu}$ mirror plane of the molecule separating the two carbon atoms. In the $C_{2\nu}$ plane, there is a symmetric axis from the minimum to the left point of the VRI belt. This last (drawn) VRI point is symmetrically between the atoms C1 and C2 with $C_{2\nu}$ symmetry. It is 5780 cm^{-1} above structure **1**. It lies on the vibrational trajectory of ν_{11}, i.e. the bridging H5 vibrates against the carbon atoms (see Fig. 3). ν_{11} acts totally symmetrically in this symmetry plane. At the back side of the minimum bowl, this mode is part of the pathway of deprotonation of the single $H5^+$.

The bifurcation of any RP from the minimum to the lower symmetry of the SPs **2** cannot be avoided. Thus, to understand any kind of RP which connects the minimum with one of the SPs **2** or **2′**, we have to understand the BPs on these pathways. The Branin method is our tool to systematically get VRI points of the PES. In Fig. 8, the bifurcation of the TASC pathway (crossing of the first two eigenvalues) as well as the GE bifurcation takes place before reaching the VRI point. However, the exact calculation of these types of BPs is an expensive luxury. The crossing of the VRI belt with the MEP is the most suitable and best available point to explain the RP bifurcation, at least in the symmetric case.

4. The planar saddle points

The planar SPs **3**–**5** are found by the new procedures described above using straight forward calculations. All five H atoms are in the molecular plane.

SP structure **3** is found by RGF starting at the minimum **1** in direction δ_5 perpendicular to the $C_{2\nu}$ symmetry plane. It lies 64.2 kcal/mol above the global

minimum. SP **3** is of index two; the second negative eigenvalue direction is the in-plane bending. The pathway from minimum **1** to SP **3** of index two has to pass a VRI point. It is located at $\delta_5 = 134°$.

The other two SPs are results of RGF pathways in the plane: the descent from SP structure **3** to the second decay direction within the plane gives **4**, again a SP of index one, already reported in Ref. [5]. SP **4** is 48.1 kcal/mol above **1**. We may imagine that it is built by a rotation of the two neighboring H atoms of SP **2** into the plane of all the remaining atoms. Starting from SP **2** and going uphill, one has to go along a ridge. Because **2** and **4** are both saddles of index one, a VRI point on the pathway between them does exist again.

In Ref. [5] it is reported that an IRC from SP **4** leads to the global minimum **1**. That is true although the IRC falls first down the slope into the valley of SP **2**. However, circumnavigating the SP **2**, the IRC further downs to the minimum **1**. It is well known that the steepest descent does not meet the corresponding SP from above (here **2**), without symmetry conservation, but passes by it and goes further downslope to the minimum. It is an example that the IRC is not attracted by the next SP in contrast to RGF [31].

A further bending of the two connected H atoms of SP **4** gives the SP **5**, which is also reached by RGF from minimum using the lowest mode along α_5, the bending of H5. Holding the symmetry after the VRI point, not one of the bifurcating branches is followed, but the ascent is further followed along the ridge. The energy of this stationary point **5** is 58.1 kcal/mol. A GE curve leads to this SP **5** as well which comes from minimum **1**. The first piece of this GE is shown above in Figs. 5, 6, and 8. The GE has a bifurcation point at $\alpha_5 = 94°$ where the side GEs coming from the SPs **2** or **2′** meet. The GE has a second bifurcation point at $\alpha_5 = 122°$. At that point, H5 and the other two hydrogens H1 and H2 form a CH_3 group. To reach the SP 5, the H5 has to bend further down into the plane of H3 and H4, as well as the H1 and H2 have to bend up also into this plane.

5. The SP of H_2 dissociation

The elimination of H_2 from organic cations is a reaction of considerable interest in chemistry. $C_2H_5^+$ has been studied with more sophisticated methods some years ago [5,6]. The SP **6** of H_2 dissociation calculated with MP2/6-31G** shows a similar geometry as reported in Ref. [5], cf. Fig. 2. It is an example of a so-called Don Quixote SP [48]. The SP **6** is characterized by a decomposition mode being larger in its absolute value than four of the residual ridge modes. Four normal modes are lower in their force constants than $|\nu_1|$, see Table 1. The decomposition mode ν_1 does not only concern the distance of the H1–H5 couple, but also concerns the angles of the remaining three H atoms, which are forming the structure of the $C_2H_3^+$, cf. [5]. So, the orography around SP **6** is quite complex. To locate the SP **6**, RGF was used started at $\alpha_5 = 122°$, i.e. at the second GE bifurcation. The RGF search direction is chosen with the direction of the side branches of the GE bifurcation. (The GE bifurcation point, see Refs. [15,16,42,49] for the theoretical background, is not available by TASC or RGF.) The example shows that the bifurcations of the α_5-GE, here at 94 and 122°, do generally not take place at the crossing point of the eigenvalues which takes place here at 89.3°, see above. This contrasts with a remark in Ref. [27]. Also the VRI point on this pathway is at a different place: at $\alpha_5 = 103°$.

6. Conclusions

The ethyl cation is used to demonstrate the workability of different algorithms (IRC, RGF, Branin's method, TASC and GE) to analyze the PES. First, the streambed GE and other MEP curves were followed to find the SPs of the H-shifts together with MEP branching. The SPs are of first index and lie on the top of a side branch GE. The pathway starts at the global minimum of the ethyl cation in the direction of the 'smallest' eigenvector (RGF, TASC, GE) and we do not use any further external knowledge to continue. (Alternately, we may also start at the SP and go downhill, as it is done with the IRC. In case of a continuous streambed the same line is obtained under TASC.) TASC requires the evaluation of the gradient and the Hessian in each step (or updates of the Hessian). The TASC is a modified RGF method comparable in its effort with the original RGF method [12–14] to determine the MEP. It is only the projector

matrix, $\mathbf{P}_{\mathbf{x}'(t)}$, with the direction $\mathbf{x}'$ of Eq. (5), which must be additionally recalculated for Eq. (3) after every predictor step. The numeric effort is next to nothing. The procedure is a potent method for studying the streambed MEPs of multidimensional surfaces as it is demonstrated in this paper for $C_2H_5^+$.

The solution of TASC is uniquely defined by the PES, actually a numeric approximation of the valley floor gradient extremal. The valley floor GE describes frequently that MEP of first chemical interest. Besides the H shift problem discussed here, one often wish to find the streambed in the conformational space of dihedral angles which represent the weakest mode in a molecule [50–53]. Direct GE calculations would be very expensive! The few selected points of the GE pathway (13 predictor steps) in Fig. 8 required one month using an HP workstation. It would require even much more, if the valley floor GE has to be separated from the other GEs which have no chemical interest. The corresponding MEP part found by TASC needs less than 30 h (for 46 predictor steps of the MEP). Thus, TASC is a very effective alternative. BPs of the streambed GE are not necessarily indicated by TASC, but the crossing of the absolute values of the first two eigenvalues forces the corrector to search (by controlled steplength) for another streambed GE in the neighborhood. It appears that the combination of RGF, TASC, and IRC can overcome a lot of limitations of the single methods in analysing the PES.

The second aim was to find further SPs surrounding the minimum bowl of the ethyl cation. This could be reached by the RGF method [12]. It was applied for **3** planar SPs of index one and two, and the known SP of the H_2 dissociation [5].

A third goal was to find and discuss symmetric BP of RGF curves which are at the same time VRI points of the PES. We located the position of a 'belt' of VRI points using the Branin method. This is the first application of the method to a larger molecule in comparison to a former study of H_2CO being a six-dimensional case with four symmetric modes [38]. The calculation of VRI points by BPs of RGF curves is found to be the best tool to handle this task. The manifold of VRI points is an unique property of the PES [21,22] and it is independent on the choice of coordinates. On the other hand: There are different MEP definitions. The crossing point of any MEP with the manifold of VRI points represents that point which we should accept as the branching point of the MEP. We have to consider that the position of such BPs on the PES may more or less differ due to different definitions of the MEP. An illustration of the VRI manifold is given in Fig. 8(b), as well as in Refs. [14,38].

Acknowledgements

Our work was made possible through the financial support of the Deutsche Forschungsgemeinschaft as well as through the help offered by the Naturwissenschaftlich-Theoretisches Zentrum der Universität Leipzig. We warmly thank M. Hirsch for many interesting discussions, and we thank the referees for some useful suggestions.

References

[1] B. Zurawski, R. Ahlrichs, W. Kutzelnigg, Chem. Phys. Lett. 21 (1973) 309.
[2] H.-J. Köhler, D. Heidrich, H. Lischka, Z. Chem. 17 (1977) 67.
[3] P.v.R. Schleyer, P. Maerker, S. Sieber, in: G.K.S. Prakash, P.v.R. Schleyer (Eds.), Stable Carbocation Chemistry, Wiley, New York, 1997, p. 33.
[4] D. Heidrich, M. Grimmer, H.-J. Köhler, Tetrahedron 32 (1976) 1193.
[5] E. del Rio, R. Lopez, T.L. Sordo, J. Phys. Chem. A 102 (1998) 6831.
[6] E. Uggerud, Eur. Mass Spectrom. 3 (1997) 403.
[7] K. Laidler, Theory of Reaction Rates, McGraw-Hill, New York, 1969.
[8] W. Miller, N.C. Handy, J.E. Adams, J. Chem. Phys. 72 (1980) 99.
[9] G.D. Billing, K.V. Mikkelsen, Advanced Molecular Dynamics and Chemical Kinetics, Wiley, New York, 1997.
[10] D.G. Truhlar, in: D. Heidrich (Ed.), The Reaction Path in Chemistry: Current Approaches and Perspectives, Kluwer Academic Publishers, Dordrecht, 1995, p. 229.
[11] W. Quapp, D. Heidrich, Theor. Chim. Acta 66 (1984) 245.
[12] W. Quapp, M. Hirsch, O. Imig, D. Heidrich, J. Comput. Chem. 19 (1998) 1087.
[13] W. Quapp, M. Hirsch, D. Heidrich, Theor. Chem. Acc. 100 (1998) 285.
[14] M. Hirsch, W. Quapp, D. Heidrich, Phys. Chem. Chem. Phys. 1 (1999) 5291.
[15] J.-Q. Sun, K. Ruedenberg, J. Chem. Phys. 98 (1993) 9707.
[16] O. Imig, W. Quapp, D. Heidrich, unpublished procedure, 1996.
[17] W. Quapp, Comp. Math. Appl. 41 (2001) 407.
[18] W. Quapp, M. Hirsch, D. Heidrich, Theor. Chem. Acc. 105 (2000) 145.

[19] W. Quapp, in: D. Heidrich (Ed.), The Reaction Path in Chemistry: Current Approaches and Perspectives, Kluwer Academic Publishers, Dordrecht, 1995, p. 95.
[20] F.H. Branin, IBM J. Res. Dev. (1972) 504.
[21] D.J. Wales, J. Chem. Phys. 113 (2000) 3926.
[22] W. Quapp, J. Chem. Phys. 114 (2001) 609.
[23] D.G. Truhlar, B.C. Garrett, Acc. Chem. Res. 13 (1980) 440.
[24] A.D. Isaacson, in: D. Heidrich (Ed.), The Reaction Path in Chemistry: Current Approaches and Perspectives, Kluwer Academic Publishers, Dordrecht, 1995, p. 191.
[25] A.G. Baboul, H.B. Schlegel, J. Chem. Phys. 107 (1997) 9413.
[26] F. Eckert, J. Werner, Theor. Chem. Acc. 100 (1998) 21.
[27] K. Ruedenberg, J.-Q. Sun, J. Chem. Phys. 100 (1994) 5836.
[28] M.F. Guest, P. Fantucci, R.J. Harrison, J. Kendric, J.H. van Lenthe, K. Schoeffel and P. Sherwood, GAMESS-UK program, CFS Ltd., Daresbury Lab., 1993.
[29] K. Fukui, J. Phys. Chem. 74 (1970) 4161.
[30] I.H. Williams, G.M. Maggiora, J. Mol. Struct. (Theochem) 89 (1982) 365.
[31] W. Quapp, J. Comput. Chem. 22 (2001) 537.
[32] D. Lauvergnat, A. Nauts, Y. Justum, X. Chapuisat, J. Chem. Phys. 114 (2001) 6592.
[33] H. Gotō, Chem. Phys. Lett. 292 (1998) 254.
[34] A.J. Turner, V. Moliner, I.H. Williams, Phys. Chem. Chem. Phys. 1 (1999) 1323.
[35] C.J. Cerjan, W.H. Miller, J. Chem. Phys. 75 (1981) 2800.
[36] D.J. Wales, J. Chem. Soc., Faraday Trans. 89 (1993) 1305.
[37] D.J. Wales, J. Chem. Phys. 101 (1994) 3750.
[38] W. Quapp, V. Melnikov, Phys. Chem. Chem. Phys. 3 (2001) 2735.
[39] M.V. Basilevsky, A.G. Shamov, Chem. Phys. 337 (1981) 347.
[40] D.K. Hoffman, R.S. Nord, K. Ruedenberg, Theor. Chim. Acta 69 (1986) 265.
[41] W. Quapp, O. Imig, D. Heidrich, in: D. Heidrich (Ed.), The Reaction Path in Chemistry: Current Approaches and Perspectives, Kluwer Academic Publishers, Dordrecht, 1995, p. 137.
[42] D. Heidrich, W. Kliesch, W. Quapp, Properties of Chemically Interesting Potential Energy Surfaces, Lecture Notes in Chemistry 56, Springer, Berlin, 1991.
[43] G. Schafternaar, MOLDEN, CAOS/CAMM Center Nijmegen Toernooiveld, 1995.
[44] C. Møller, M.S. Plesset, Phys. Rev. 46 (1934) 618.
[45] D. Heidrich, M. Stromeyer, Z. Chem. 16 (1976) 153.
[46] T.H. Choi, S.T. Park, M.S. Kim, J. Chem. Phys. 114 (2001) 6051.
[47] Ch. Aubery, J.L. Holmes, J. Phys. Chem. A 102 (1998) 6441.
[48] P.G. Mezey, Potential Energy Hypersurfaces, Elsevier, Amsterdam, 1987.
[49] M.V. Basilevsky, Theor. Chim. Acta 72 (1987) 63.
[50] L.N. Santana, F.D. Suvire, R.D. Enriz, L.L. Torday, I.G. Csizmadia, J. Mol. Struct. (Theochem) 465 (1999) 33.
[51] I. Kolossváry, W.C. Guida, J. Comput. Chem. 20 (1999) 1671.
[52] D. ben-Avraham, M.M. Tirion, Physica A 249 (1998) 415.
[53] H. Gotō, J. Mol. Struct. (Theochem) 285 (1993) 157.